Nuclear Engineering and Technology 49 (2017) 1019–1030

Contents lists available at ScienceDirect

Nuclear Engineering and Technology

journal homepage: www.elsevier.com/locate/net

Original Article

An innovative method for determining the diffusion coefficient of product nuclide

Chih-Lung Chen [a, *], Tsing-Hai Wang [b]

[a] Department of Nuclear Back-end Management, Taiwan Power Company, Taipei, Taiwan
[b] Department of Biomedical Engineering and Environment Sciences, National Tsing Hua University, Hsinchu, Taiwan

ARTICLE INFO

Article history:
Received 1 December 2016
Received in revised form
29 March 2017
Accepted 29 March 2017
Available online 11 July 2017

Keywords:
Diffusion Coefficient
Sequentially Reactive
Through-Diffusion

ABSTRACT

Diffusion is a crucial mechanism that regulates the migration of radioactive nuclides. In this study, an innovative numerical method was developed to simultaneously calculate the diffusion coefficient of both parent and, afterward, series daughter nuclides in a sequentially reactive through-diffusion model. Two constructed scenarios, a serial reaction (RN_1 → RN_2 → RN_3) and a parallel reaction (RN_1 → RN_2A + RN_2B), were proposed and calculated for verification. First, the accuracy of the proposed three-member reaction equations was validated using several default numerical experiments. Second, by applying the validated numerical experimental concentration variation data, the as-determined diffusion coefficient of the product nuclide was observed to be identical to the default data. The results demonstrate the validity of the proposed method. The significance of the proposed numerical method will be particularly powerful in determining the diffusion coefficients of systems with extremely thin specimens, long periods of diffusion time, and parent nuclides with fast decay constants.

1. Introduction

The diffusion of nuclides into a rock matrix is one of the main mechanisms retarding migration from a repository [1]. Numerous laboratory-based methods have been proposed to determine diffusion coefficients [2,3]. Among these methods, the two-reservoir through-diffusion method is frequently used, in which the geological media (i.e., the specimen) is sandwiched between two reservoirs, one reservoir including the nuclide (the source term) and the other nuclide-free (the end term). The source term is known as an upstream reservoir (UR), and the end term is known as a downstream reservoir (DR).

Depending on the design of the two-reservoir through-diffusion experiment, the concentration in the source term can be fixed (i.e., a constant concentration source) or varied (i.e., a variable concentration source). Similarly, the concentration in the end term can also be fixed or varied. An overview of diffusion experiment and analysis methods has been performed [2,3]. Recently, a systematic evaluation regarding the potential problems associated with conventional laboratory diffusion and batch experiments has been conducted [4]. Rigorous solutions to the through-diffusion tests have been developed and discussions on how to select the most appropriate test method, optimization of the test conditions, and data sampling for the through-diffusion tests have been conducted [4,5]. Significant improvements in the laboratory diffusion tests have also been achieved [6,7]. Based on the above advances [4], four combinations that are capable of determining diffusion coefficients in the most effective manner are suggested, including a constant inlet concentration–constant outlet concentration (CC–CC) model [4,8,9], a constant inlet concentration–variable outlet concentration (CC–VC) model [4,10,11], a variable inlet concentration–constant outlet concentration (VC–CC) model [4,8], and a variable inlet concentration–variable outlet concentration (VC–VC) model [4,12–14].

The mass balance equation was used in the CC–CC model to derive the total quantity by considering the effective cross area at the downstream boundary. By assuming $t \to \infty$, an asymptotic solution to determine the diffusion coefficient of a parent nuclide was developed [8]. An asymptotic solution was also suggested to estimate the diffusion coefficient in the CC–VC model [10]. The VC–CC model has been only rarely discussed or used. The popular VC–VC model was based on the continuous transport model and is used for discussing the variations of nuclide concentration in the UR, specimen, and DR [12]. An analytical solution, with the assumption of

* Corresponding author.
E-mail address: chencl@iner.gov.tw (C.-L. Chen).

http://dx.doi.org/10.1016/j.net.2017.03.011

linear sorption of the VC–VC model, was obtained [7]. A compartmental method with the explicit scheme and the Crank–Nicolson scheme of the finite derivation numerical method were used; the formulas accounting for the nuclide concentration variations in the UR, the specimen, and the DR were determined in the time domain of the VC–VC model [13]. A method of determining the diffusion coefficient of the VC–VC model, which takes the decay effect into account, was proposed [14].

Whereas all the aforementioned studies have mainly focused on determining the diffusion coefficient of a single parent nuclide, the issue of a daughter nuclide decaying from a parent nuclide has received less attention. Developing a feasible method for determining the diffusion coefficient of a product nuclide is therefore highly desired as it will allow not only a reduction of radwaste production but also a considerable saving of experimental time. These are the incentives that have initialized this study: we propose a method that considers three-member reactive nuclide diffusion transport equations in serial and parallel reactions of continuous and compartmental models for the cross-validation and verification of the method used to determine the diffusion coefficient.

2. Mathematical model

2.1. Continuum model

A one-dimensional diffusion equation derived from the mass balance was used to describe the solute diffusion transport in a uniform continuum porous medium.

$$D_m\frac{\partial^2 C}{\partial x^2}-\frac{\rho_b}{n}\frac{\partial S}{\partial t}=\frac{\partial C}{\partial t}, \tag{1}$$

where

C solute concentration in the pore water (M/L^3)
D_m intrinsic diffusion coefficient in the pore water (L^2/T)
S mass of the solute adsorbed per unit bulk dry mass of porous medium (−)
n porosity of the porous medium (−)
ρ_b bulk dry density of the porous medium (M/L^3)
x length coordinates (L)
t time (T)

The first term on the left-hand side of Eq. (1) describes the diffusion in the mobile pore water. The second term describes the solute adsorbed by the medium. The term on the right-hand side describes the accumulation of the solute.

The sorption of each member nuclide is assumed to be linear reversible and instantaneous. The linear relationship can be presented as $S=K_dC$, where K_d is the distribution coefficient (L^3/M). Eq. (1) can be reduced to:

$$D_m\frac{\partial^2 C}{\partial x^2}=\frac{\partial C}{\partial t}\left(1+\frac{\rho_b}{n}K_d\right) \tag{2}$$

or

$$D\frac{\partial^2 C}{\partial x^2}=\frac{\partial C}{\partial t}, \tag{3}$$

where D is the apparent diffusion coefficient [L^2/T; D can be expressed as $D=\frac{D_m}{R}$, where $R=1+\frac{\rho_b}{n}K_d$ is the retardation factor (−)].

Considering that the condition of the solute is a radioactive nuclide, Eq. (3) adds a decay term and becomes:

$$D\frac{\partial^2 C}{\partial x^2}-\lambda C=\frac{\partial C}{\partial t}, \tag{4}$$

where λ is the decay constant [1/T; which can be expressed as $\lambda=\ln(2)/H_f$, where H_f is the half-life (T)].

Based on the aforementioned considerations, the diffusion transport of multiple nuclide decay chains is given by:

$$D_i\frac{\partial^2 C_i}{\partial x^2}-\lambda_i C_i+y_i\lambda'_{i-1}C_{i-1}=\frac{\partial C_i}{\partial t},\quad \forall\ i=1,2,\ldots,n \tag{5}$$

where

C_i ith nuclide concentration in the pore water (M/L^3)
C_{i-1} parent nuclide concentration of the ith nuclide in the pore water (M/L^3)
D_i apparent diffusion coefficient of the ith nuclide in the pore water (L^2/T)
y_i stoichiometric yield factor (−)
λ_i decay constant of ith nuclide (1/T)

λ'_{i-1} can be expressed as $\frac{R_{i-1}}{R_i}\lambda_{i-1}$, where λ_{i-1} is the decay constant of the parent nuclide of the ith nuclide (1/T); R_i and R_{i-1} are the retardation factors (−) of the ith nuclide and its parent nuclide, respectively.

In this study, the diffusion phenomenon was considered to occur in two reservoirs within a geological material specimen (Fig. 1). The initial conditions of the serial reactions are:

$$\begin{cases} C_i(x,t=0)=0 \\ C_{UR,i}(t=0)=C_{o,i} \\ C_{DR,i}(t=0)=0 \end{cases}, \tag{6}$$

where UR and DR represent the upstream reservoir and the downstream reservoir, respectively, and $C_{o,i}$ describes the initial concentrations of the ith nuclide in the UR.

The boundary conditions are considered separately in the UR and DR.

In UR ($x=0$),

$$\begin{cases} C_i(x=0,t)=C_{UR,i}(t) & \ldots(A) \\ V_{IR}\dfrac{dC_{UR,i}}{dt}=V_{UR}y_i\lambda_{i-1}C_{UR,i-i}-V_{UR}\lambda_i C_{UR,i}+A_eD_i\dfrac{\partial C_i}{\partial x}\Big|_{x=0} & \ldots(B) \end{cases}, \tag{7}$$

where V_{UR} is the volume of UR (L^3) and A_e is the effective diffusion cross section [L^2; which can be expressed as $A_e=nA$, where A is the cross section of the specimen (L^2)].

In DR ($x=L$),

$$\begin{cases} C_i(x=L,t)=C_{DR,i}(t) & \ldots(A) \\ V_{DR}\dfrac{dC_{DR,i}}{dt}=V_{DR}y_i\lambda_{i-1}C_{DR,i-1}-V_{DR}\lambda_i C_{DR,i}-A_eD_i\dfrac{\partial C_i}{\partial x}\Big|_{x=L} & \ldots(B) \end{cases}, \tag{8}$$

where V_{DR} is the volume of DR (L^3) and L is the thickness of the specimen (L).

For practical analysis and discussion, the three-member reaction was considered.

2.1.1. Serial reactions

The three-member serial reaction is shown in Fig. 2. In this case, the stoichiometric yield factors (y_i) are equal to 1. The

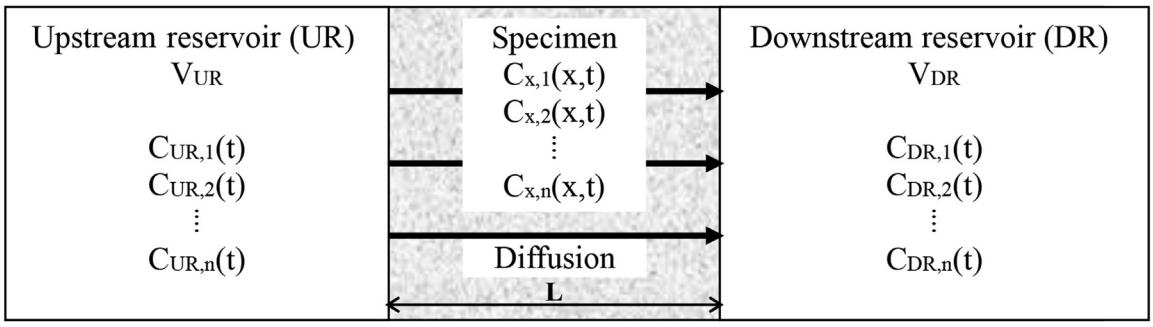

Fig. 1. Schematic layout of the multiple-nuclide through-diffusion model.

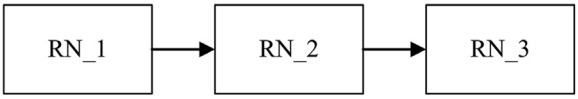

Fig. 2. Schematic layout of the three-member serial reactions (RN_1, RN_2 and RN_3 are parent nuclide, daughter nuclide and its product nuclide, respectively).

concentration solutions of the first two members in the Laplace domain were reported as follows [14].

The parent nuclide (RN_1):

$$\overline{C}_{UR,1}(p) = \frac{M_2 V_{UR} C_{o,1}}{(p+\lambda_1)M_2 V_{UR} - (p+\lambda_1)M_1 V_{DR}} \tag{9}$$

$$\overline{C}_{x,1}(x,p) = \frac{V_A C_{o,1}}{(p+\lambda_1)M_2 V_{UR} - (p+\lambda_1)M_1 V_{DR}} [M_2 \cosh(m_1 x) + \sinh(m_1 x)] \tag{10}$$

$$\overline{C}_{DR,1}(p) = \frac{V_{UR} C_{o,1}}{(p+\lambda_1)M_2 V_{UR} - (p+\lambda_1)M_1 V_{DR}} [M_2 \cosh(m_1 L) + \sinh(m_1 L)] \tag{11}$$

where $M_2 = -\frac{M_1 \cosh(m_1 L)+\sinh(m_1 L)}{M_1 \sinh(m_1 L)+\cosh(m_1 L)}$, $M_1 = \frac{m_1 A_e D_1}{V_{DR}(p+\lambda_1)}$ and $m_1 = \sqrt{\frac{p+\lambda_1}{D_1}}$. A bar over a function designates its Laplace transform in terms of t.

The first product nuclide (RN_2):

$$\overline{C}_{UR,2}(p) = B_1 + \frac{\alpha M_2}{m_1^2 - m_2^2} \tag{12}$$

$$\overline{C}_{x,2}(x,p) = B_1 \cosh(m_2 x) + B_2 \sinh(m_2 x) + \frac{\alpha}{m_1^2 - m_2^2} [M_2 \cosh(m_1 x) + \sinh(m_1 x)] \tag{13}$$

$$\overline{C}_{DR,2}(p) = B_1 \cosh(m_2 L) + B_2 \sinh(m_2 L) + \frac{\alpha}{m_1^2 - m_2^2} [M_2 \cosh(m_1 L) + \sinh(m_1 L)] \tag{14}$$

where

$\alpha = \frac{-\lambda_1' V_{UR} C_{o,1}}{(p+\lambda_1)(M_2 V_{UR} - M_1 V_{DR})}$; $m_2 = \sqrt{\frac{p+\lambda_2}{D_2}}$; $B_1 = \frac{\gamma_1 \chi_3 - \gamma_3 \chi_1}{\gamma_1 \chi_2 - \gamma_2 \chi_1}$; $B_2 = \frac{\gamma_2 \chi_3 - \gamma_3 \chi_2}{\gamma_2 \chi_1 - \gamma_1 \chi_2}$

$\gamma_1 = V_A (p+\lambda_2)$; $\gamma_2 = -m_2 A_e D_2$

$$\gamma_3 = \frac{-\alpha M_2 V_{UR}(p+\lambda_2)}{m_1^2 - m_2^2} + V_{UR}\left(C_{o,2} + \lambda_1 \overline{C}_{UR,1}\right) + \frac{\alpha m_1 A_e D_2}{m_1^2 - m_2^2};$$

$\chi_1 = V_{DR}(p+\lambda_2)\cosh(m_2 L) + m_2 A_e D_2 \sinh(m_2 L)$;

$\chi_2 = V_{DR}(p+\lambda_2)\sinh(m_2 L) + m_2 A_e D_2 \cosh(m_2 L)$

$$\chi_3 = V_{DR}\lambda_1 \overline{C}_{DR,1} - \frac{\alpha}{m_1^2 - m_2^2}\{V_{DR}(p+\lambda_2)[M_2 \cosh(m_1 L) + \sinh(m_1 L)] + m_1 A_e D_2 [M_2 \sinh(m_1 L) + \cosh(m_1 L)]\}$$

Following the same procedure, the concentration solution of the second product nuclide (RN_3) can be obtained as follows:

$$\overline{C}_{UR,3}(p) = E_1 + \frac{\lambda_2' B_1}{(m_3^2 - m_2^2)} + \frac{\alpha \lambda_2' M_2}{(m_1^2 - m_2^2)(m_3^2 - m_1^1)} \tag{15}$$

$$\overline{C}_{x,3}(x,p) = E_1 \cosh(m_3 x) + E_2 \sinh(m_3 x) + \frac{\lambda_2'}{(m_3^2 - m_2^2)} [B_1 \cosh(m_2 x) + B_2 \sinh(m_2 x)] + \frac{\alpha \lambda_2'}{(m_1^2 - m_2^2)(m_3^2 - m_1^2)} [M_2 \cosh(m_1 x) + \sinh(m_1 x)] \tag{16}$$

$$\overline{C}_{DR,3}(p) = E_1 \cosh(m_3 L) + E_2 \sinh(m_3 L) + \frac{\lambda_2'}{(m_3^2 - m_2^2)} [B_1 \cosh(m_2 L) + B_2 \sinh(m_2 L)] + \frac{\alpha \lambda_2'}{(m_1^2 - m_2^2)(m_3^2 - m_1^2)} [M_2 \cosh(m_1 L) + \sinh(m_1 L)] \tag{17}$$

where

$m_3 = \sqrt{\frac{p+\lambda_3}{D_3}}$; $E_1 = \frac{\delta_2 \kappa_3 - \delta_3 \kappa_3}{\delta_2 \kappa_1 - \delta_1 \kappa_2}$; $E_2 = \frac{\delta_1 \kappa_3 - \delta_3 \kappa_1}{\delta_1 \kappa_2 - \delta_2 \kappa_1}$;

$\delta_1 = V_{UR}(p+\lambda_3)$; $\delta_2 = -m_3 A_e D_3$;

$$\delta_3 = V_{UR}\left(C_{o,3} + \lambda_2 \overline{C}_{UR,2}\right) + \frac{\lambda_2'}{m_3^2 - m_2^2}[A_e D_3 B_2 m_2 - V_{UR}(p+\lambda_3)B_1] + \frac{\alpha \lambda_2'}{(m_1^2 - m_2^2)(m_3^2 - m_1^2)}[A_e D_3 m_1 - V_{UR}(p+\lambda_3)M_2];$$

$$\kappa_1 = V_{DR}(p+\lambda_3)\cosh m_3 L + m_3 A_e D_3 \sinh m_3 L;$$

$$\kappa_2 = V_{DR}(p+\lambda_3)\sinh m_3 L + m_3 A_e D_3 \cosh m_3 L;$$

$$\kappa_3 = V_{DR}\lambda_2 \overline{C}_{DR,2} - \frac{\lambda_2'}{(m_3^2 - m_2^2)}\{[V_{DR}(p+\lambda_3)B_1 + A_e D_3 B_2 m_2]\cosh(m_2 L) + [V_{DR}(p+\lambda_3)B_2 + A_e D_3 B_1 m_2]\sinh(m_2 L)\} - \frac{\alpha\lambda_2'}{(m_1^2 - m_2^2)(m_3^2 - m_1^2)} \times \{[V_{DR}(p+\lambda_3)M_2 + A_e D_3 m_1]\cosh(m_1 L) + [V_{DR}(p+\lambda_3) + A_e D_3 N m_1]\sinh(m_1 L)\}$$

2.1.2. Parallel reactions

The three-member parallel reaction is shown in Fig. 3. In this case, the stoichiometric yield factors are not equal to 1 and must be considered. The concentration variation of the parent nuclide is the same as that in the serial reaction; however, the concentration solution of the daughter nuclide changes. Using the Laplace transform method, the concentration solution of the first branch nuclide (RN_2A) can be derived as follows:

$$\overline{C}_{UR,2A}(p) = B_{1A} + \frac{\alpha_A M_2}{m_1^2 - m_{2A}^2} \tag{18}$$

$$\overline{C}_{x,2A}(x,p) = B_{1A}\cosh(m_{2A}x) + B_{2A}\sinh(m_{2A}x) + \frac{\alpha_A}{m_1^2 - m_{2A}^2}[M_2\cosh(m_1 x) + \sinh(m_1 x)] \tag{19}$$

$$\overline{C}_{DR,2A}(p) = B_{1A}\cosh(m_{2A}L) + B_{2A}\sinh(m_{2A}L) + \frac{\alpha_A}{m_1^2 - m_{2A}^2}[M_2\cosh(m_1 L) + \sinh(m_1 L)] \tag{20}$$

where

$\alpha_A = \frac{-\lambda_{1A}' V_{UR} C_{o,1}}{(p+\lambda_1)(M_2 V_{UR} - M_1 V_{DR})}$; $m_{2A} = \sqrt{\frac{p+\lambda_{2A}}{D_{2A}}}$; $\lambda_{1A}' = \frac{R_1}{R_2}\lambda_1 y_A$;

$$B_{1A} = \frac{\gamma_1\chi_{3A} - \gamma_{3A}\chi_1}{\gamma_1\chi_2 - \gamma_2\chi_1};\ B_{2A} = \frac{\gamma_2\chi_{3A} - \gamma_{3A}\chi_2}{\gamma_2\chi_1 - \gamma_1\chi_2};$$

$$\gamma_{3A} = \frac{-\alpha_A M_2 V_{UR}(p+\lambda_{2A})}{m_1^2 - m_{2A}^2} + V_{IR}\left(C_{o,2A} + y_A\lambda_1\overline{C}_{UR,1}\right) + \frac{\alpha_A m_1 A_e D_{2A}}{m_1^2 - m_{2A}^2};$$

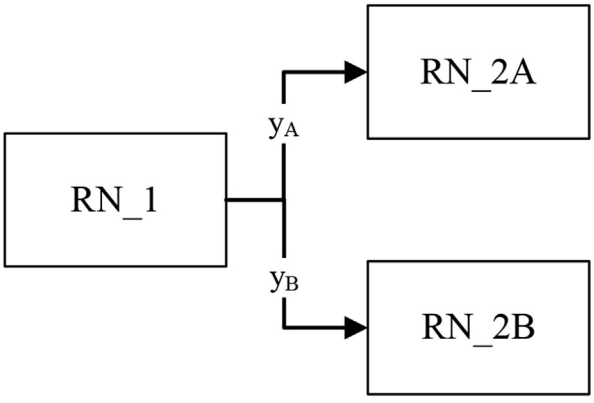

Fig. 3. Schematic layout of the three-member parallel reactions (RN_2A and RN_2B are branch daughter nuclides, respectively).

$$\chi_{3A} = y_A V_{DR}\lambda_1\overline{C}_{DR,1} - \frac{\alpha_A}{m_1^2 - m_{2A}^2}\{V_{DR}(p+\lambda_{2A})[N\cosh(m_1 L) + \sinh(m_1 L)] + m_1 A_e D_{2A}[N\sinh(m_1 L) + \cosh(m_1 L)]\}$$

where $C_{o,2A}$ is the initial concentration of the first branch nuclide in the UR.

Similarly, if we substitute the properties of the second branch nuclide (RN_2B) for RN_2A, and the concentration solution of RN_2B can be obtained from Eqs. (18–20).

2.2. Compartmental model

Considering the multiple nuclide decay chains with one compartment of the specimen in the two-reservoir through-diffusion model, the concentration equations can be derived using the finite difference method, as follows:

$$V_{UR}\frac{dC_{UR,i}}{dt} = y_i\lambda_{i-1}V_{UR}C_{A,i-1} - \lambda_i V_{UR}C_{A,i} + A_e D_i\frac{(C_{s,i} - C_{UR,i})}{L/2} \tag{21}$$

$$V_s\frac{dC_{s,i}}{dt} = y_i\lambda_{i-1}V_s C_{s,i-1} - \lambda_i V_s C_{s,i} + A_e D_i\frac{(C_{DR,i} - C_{s,i})}{L/2} - A_e D_i\frac{(C_{s,i} - C_{UR,i})}{L/2} \tag{22}$$

$$V_{DR}\frac{dC_{DR,i}}{dt} = y_i\lambda_{i-1}V_{DR}C_{DR,i-1} - \lambda_i V_{DR}C_{DR,i} - A_e D_i\frac{(C_{DR,i} - C_{s,i})}{L/2}, \tag{23}$$

where $C_{s,i}$ represents the ith nuclide concentration in the specimen (M/L^3); V_s is the effective volume of the specimen (L^3; which can be expressed as $V_s = A_e L$).

The Laplace transform method was used to solve the three-member reaction solutions of serial and parallel reactions.

2.2.1. Serial reactions

In this case, the stoichiometric yield factors (y_i) are set to 1. The concentration solutions of the first two members of the compartmental model in the Laplace domain were presented as follows [14]:

the parent nuclide (RN_1):

$$\overline{C}_{UR,1} = \frac{V_{UR}C_{o,1}}{[2\alpha_1 + (p+\lambda_1)V_{UR}] - \frac{(2\alpha_1)^2}{[4\alpha_1 + (p+\lambda_1)V_s] - \frac{(2\alpha_1)^2}{2\alpha_1 + (p+\lambda_1)V_{DR}}}} \tag{24}$$

$$\overline{C}_{s,1} = \frac{2\alpha_1}{[4\alpha_1 + (p+\lambda_1)V_s] - \frac{(2\alpha_1)^2}{2\alpha_1 + (p+\lambda_1)V_{DR}}}\overline{C}_{UR,1} \tag{25}$$

$$\overline{C}_{DR,1} = \frac{2\alpha_1}{2\alpha_1 + (p+\lambda_1)V_{DR}}\overline{C}_{s,1} \tag{26}$$

where $\alpha_1 = \frac{A_e D_1}{L}$.

The first product nuclide (RN_2):

$$\overline{C}_{UR,2} = \frac{V_{UR}C_{o,2}}{2\alpha_2 + (p+\lambda_2)V_{UR} - 2\alpha_2 E_{22}} + \frac{\lambda_1 V_{UR}\overline{C}_{UR,1} + 2\alpha_2 F_{22}}{2\alpha_2 + (p+\lambda_2)V_{UR} - 2\alpha_2 E_{22}} \tag{27}$$

$$\overline{C}_{s,2} = \frac{2\alpha_2}{[4\alpha_2 + (p+\lambda_1)V_s] - 2\alpha_2 E_{21}}\overline{C}_{UR,2} + \frac{\lambda'_1 V_s \overline{C}_{s,1} + 2\alpha_2 F_{21}}{[4\alpha_2 + (p+\lambda_1)V_s] - 2\alpha_2 E_{21}} \quad (28)$$

$$\overline{C}_{DR,2} = \frac{2\alpha_2}{[2\alpha_2 + (p+\lambda_2)V_{DR}]}\overline{C}_{s,2} + \frac{\lambda_1 V_{DR}}{[2\alpha_2 + (p+\lambda_2)V_{DR}]}\overline{C}_{DR,1} \quad (29)$$

where $\alpha_2 = \frac{A_e D_2}{L}$; $E_{21} = \frac{2\alpha_2}{[2\alpha_2+(p+\lambda_2)V_{DR}]}$; $F_{21} = \frac{\lambda_1 V_{DR}}{[2\alpha_2+(p+\lambda_2)V_{DR}]}\overline{C}_{DR,1}$; $E_{21} = \frac{2\alpha_2}{[4\alpha_2+(p+\lambda_1)V_s]-2\alpha_2 E_{21}}$; $F_{22} = \frac{\lambda'_1 V_s \overline{C}_{s,1}+2\alpha_2 F_{21}}{[4\alpha_2+(p+\lambda_1)V_s]-2\alpha_2 E_{21}}$.

Following a similar process (i.e., using the Laplace transform method), the concentration solution of the second product nuclide (RN_3) can be derived as follows:

$$\overline{C}_{UR,3} = \frac{V_{UR}C_{o,3}}{2\alpha_3 + (p+\lambda_3)V_{UR} - 2\alpha_3 E_{32}} + \frac{\lambda_2 V_{UR}\overline{C}_{UR,2} + 2\alpha_3 F_{32}}{2\alpha_3 + (p+\lambda_3)V_{UR} - 2\alpha_3 E_{32}} \quad (30)$$

$$\overline{C}_{s,3} = \frac{2\alpha_3}{[4\alpha_3 + (p+\lambda_3)V_s] - 2\alpha_3 E_{31}}\overline{C}_{UR,3} + \frac{\lambda'_2 V_s \overline{C}_{s,2} + 2\alpha_3 F_{31}}{[4\alpha_3 + (p+\lambda_3)V_s] - 2\alpha_3 E_{31}} \quad (31)$$

$$\overline{C}_{DR,3} = \frac{2\alpha_3}{[2\alpha_3 + (p+\lambda_3)V_{DR}]}\overline{C}_{s,3} + \frac{\lambda_2 V_{DR}}{[2\alpha_3 + (p+\lambda_3)V_{DR}]}\overline{C}_{DR,2} \quad (32)$$

where $\alpha_3 = \frac{A_e D_3}{L}$; $E_{31} = \frac{2\alpha_3}{[2\alpha_3+(p+\lambda_3)V_{DR}]}$; $F_{31} = \frac{\lambda_2 V_{DR}}{[2\alpha_3+(p+\lambda_3)V_{DR}]}\overline{C}_{DR,2}$; $E_{32} = \frac{2\alpha_3}{[4\alpha_3+(p+\lambda_3)V_s]-2\alpha_3 E_{31}}$; $F_{32} = \frac{\lambda'_2 V_s \overline{C}_{s,2}+2\alpha_3 F_{31}}{[4\alpha_3+(p+\lambda_3)V_s]-2\alpha_3 E_{31}}$.

2.2.2. Parallel reactions

In this case, the concentration of the parent nuclide is the same as that in the serial reaction; however, the concentration of the daughter nuclide changes with the stoichiometric yield factors. The concentration solution of the first branch nuclide (RN_A) in the compartmental model can be derived as follows:

$$\overline{C}_{UR,2A} = \frac{V_{UR}C_{o,2A}}{[2\alpha_{2A} + (p+\lambda_{2A})V_{UR}] - 2\alpha_{2A}E_{22}} + \frac{y_A\lambda_1 V_{UR}\overline{C}_{IR,1} + 2\alpha_{2A}F_{22}}{[2\alpha_{2A} + (p+\lambda_{2A})V_{UR}] - 2\alpha_{2A}E_{22}} \quad (33)$$

$$\overline{C}_{s,2A} = \frac{2\alpha_{2A}}{[4\alpha_{2A} + (p+\lambda_1)V_s] - 2\alpha_{2A}E_{21}}\overline{C}_{UR,2A} + \frac{y_A\lambda'_1 V_s\overline{C}_{s,1} + 2\alpha_{2A}F_{21}}{[4\alpha_{2A} + (p+\lambda_1)V_s] - 2\alpha_{2A}E_{21}} \quad (34)$$

$$\overline{C}_{DR,2A} = \frac{2\alpha_{2A}}{[2\alpha_{2A} + (p+\lambda_{2A})V_{DR}]}\overline{C}_{s,2A} + \frac{y_A\lambda_1 V_{DR}}{[2\alpha_{2A} + (p+\lambda_{2A})V_{DR}]}\overline{C}_{DR,1} \quad (35)$$

where $\alpha_{2A} = \frac{A_e D_{2A}}{L}$; $E_{21} = \frac{2\alpha_{2A}}{[2\alpha_{2A}+(p+\lambda_{2A})V_{DR}]}\overline{C}_{s,2A}$; $F_{21} = \frac{y_A\lambda_1 V_{DR}}{[2\alpha_{2A}+(p+\lambda_{2A})V_{DR}]}\overline{C}_{DR,1}$; $\overline{C}_{UR,2A} = \frac{2\alpha_{2A}}{[4\alpha_{2A}+(p+\lambda_1)V_s]-2\alpha_{2A}E_{21}}$; $F_{22} = \frac{y_A\lambda'_1 V_s\overline{C}_{s,1}+2\alpha_{2A}F_{21}}{[4\alpha_{2A}+(p+\lambda_1)V_s]-2\alpha_{2A}E_{21}}$.

The concentration equation of the second branch nuclide (RN_2B) can be obtained by replacing the property of RN_2A with RN_2B in the above equations.

2.3. Estimation of D_i

No determination of the diffusion coefficient of the product nuclide in sequential reactions has been reported in the literature. The proposed method is described in this section.

First, according to the characteristics of the compartmental model, one can subtract Eq. (23) from Eq. (21). The value D_i is obtained using the relationship between the concentration variation and its change rate with time in the UR and DR. The equation is as follows:

$$D_i = \frac{L}{2A_e}\frac{y_i\lambda_{i-1}(V_{UR}C_{IR,i-1} - V_{DR}C_{DR,i-1}) - \lambda_i(V_{UR}C_{IR,i} - V_{DR}C_{DR,i}) - \left(V_{UR}\frac{dC_{UR,i}}{dt} - V_{DR}\frac{dC_{DR,i}}{dt}\right)}{(C_{UR,i} - C_{DR,i})} \quad (36)$$

Thus, according to Eq. (36), a constant slope of the plot of $(C_{UR,i} - C_{DR,i})$ against $y_i\lambda_{i-1}(V_{UR}C_{IR,i-1} - V_{DR}C_{DR,i-1}) - \lambda_i(V_{UR}C_{IR,i} - V_{DR}C_{DR,i}) - \left(V_{UR}\frac{dC_{UR,i}}{dt} - V_{DR}\frac{dC_{DR,i}}{dt}\right)$ can be obtained.

For the continuum model, if the specimen is thinner or the concentration gradient on both sides of the specimen approaches the same value, the boundary conditions of Eq. (7) (B) and Eq. (8) (B) can be simplified to Eqs. (21) and (23), respectively. Consequently, the same D_i relationship can be obtained.

As mentioned above, the three-member reactions are discussed in the following section. Here, the estimated equation of D_i for each nuclide in serial and parallel reactions is derived.

The serial reaction is:

$$D_1 = \frac{L}{2A_e}\frac{-\lambda_1(V_{UR}C_{UR,1} - V_{DR}C_{DR,1}) - \left(V_{UR}\frac{dC_{UR,1}}{dt} - V_{DR}\frac{dC_{DR,1}}{dt}\right)}{(C_{UR,1} - C_{DR,1})} \quad (37)$$

$$D_2 = \frac{L}{2A_e}\frac{\lambda_1(V_{UR}C_{UR,1} - V_{DR}C_{DR,1}) - \lambda_2(V_{UR}C_{UR,2} - V_{DR}C_{DR,2}) - \left(V_{UR}\frac{dC_{UR,2}}{dt} - V_{DR}\frac{dC_{DR,2}}{dt}\right)}{(C_{UR,2} - C_{DR,2})} \quad (38)$$

$$D_3 = \frac{L}{2A_e}\frac{\lambda_2(V_{UR}C_{UR,2} - V_{DR}C_{DR,2}) - \lambda_3(V_{UR}C_{UR,3} - V_{DR}C_{DR,3}) - \left(V_{UR}\frac{dC_{UR,3}}{dt} - V_{DR}\frac{dC_{DR,3}}{dt}\right)}{(C_{UR,3} - C_{DR,3})} \quad (39)$$

The parallel reaction is:

$$D_{2A} = \frac{L}{2A_e}\frac{y_A\lambda_1(V_{UR}C_{UR,1} - V_{DR}C_{DR,1}) - \lambda_2(V_{UR}C_{UR,2} - V_{DR}C_{DR,2}) - \left(V_{UR}\frac{dC_{UR,2}}{dt} - V_{DR}\frac{dC_{DR,2}}{dt}\right)}{(C_{UR,2} - C_{DR,2})} \quad (40)$$

3. Theoretical verification and discussion

3.1. Serial reactions

In this section, the accuracy of the solutions of the three-member serial reaction is verified by numerical software GoldSim with the default values of Case_S, as shown in Table 1. GoldSim (GoldSim Technology Group, https://www.goldsim.com/Home/) is commercial software for radwaste disposal safety assessment. The default data are the generic data, which are often encountered in the laboratory. The concentrations of the reactive nuclides in the UR and DR are calculated using Eqs. (24–30) for the compartmental model and Eqs. (9–17) for the continuum model. The nuclide concentration variations are illustrated in Fig. 4A. Fig. 4A shows that the nuclide concentration variations predicted by the present solutions are highly consistent between the GoldSim model, the compartmental model, and the continuum model. The RN_1 concentration in the UR decreases rapidly at a decay constant of 1E−4 1/d. Because the default value of D_1 is only 1E−4 cm^2/d, RN_1 rarely diffuses through the specimen. Thus, the RN_1 concentration in the DR increases slowly. By contrast, RN_2 has a higher diffusion coefficient than RN_1. The RN_2 concentrations in the UR and DR are approximately the same and decrease rapidly at a high decay constant of 1E−3 1/d. RN_3, with the lowest diffusion coefficient in these nuclides causes an obvious concentration difference of RN_3 in the UR and DR. During the default practical experimental period (4,000 days), the RN_3 concentration in the UR and DR shows an increasing trend. This is because the decay constant of RN_3 is only 1E−7 1/d. In addition, the decay property of RN_3 causes the total mass to be almost constant during the experimental period. The nuclide concentration variation in the UR and DR confirms the serial reactive diffusion phenomenon. These results validate the accuracy of the present solutions.

The concentration data were then used in a numerical through-diffusion experiment to demonstrate that the method for estimating the diffusion coefficient of the serial reaction proposed [i.e., Eqs. (37–39)] in this study is feasible. According to Eqs. (37–39), the diffusion coefficient of the parent nuclide can be estimated using the linear relationship between $(C_{UR,1} - C_{DR,1})$ and $-\lambda_1(V_{UR}C_{UR,1} - V_{DR}C_{DR,1}) - \left(V_{UR}\frac{dC_{UR,1}}{dt} - V_{DR}\frac{dC_{DR,1}}{dt}\right)$. Thus, these data were plotted in Fig. 4B, and a constant slope value was obtained. Similarly, we plotted the linear data for RN_2 by using Eq. (38) in Fig. 4C and RN_3 by using Eq. (39) in Fig. 4D. The estimated diffusion coefficients are listed in Table 2. The deviation of D_1 is only 0.61%. The estimated D_2 completely coincides with the default

Table 1
Default values used in this study.

	L (cm)	A_e (cm^2)	V_A (cm^3)	V_B (cm^3)	Δt (d)	RN_1		RN_2		RN_3	
						D_1 (cm^2/d)	λ_1 (1/d)	D_2 (cm^2/d)	λ_2 (1/d)	D_3 (cm^2/d)	λ_3 (1/d)
Case_S	0.1	5	100	100	30	1E−4	1E−4	1E−2	1E−3	1E−6	1E−7
Case_dt−					7						
Case_dt+					60						
Case_L−	0.05				30						
Case_L+	0.2										

	L (cm)	A_e (cm^2)	V_A (cm^3)	V_B (cm^3)	Δt (d)	RN_1		RN_2A			RN_2B		
						D_1 (cm^2/d)	λ_1 (1/d)	y_A	D_{2A} (cm^2/d)	λ_{2A} (1/d)	y_B	D_{2B} (cm^2/d)	λ_{2B} (1/d)
Case_P	0.1	5	100	100	30	1E−6	1E−4	0.1	1E−4	1E−3	0.9	1E−2	1E−7

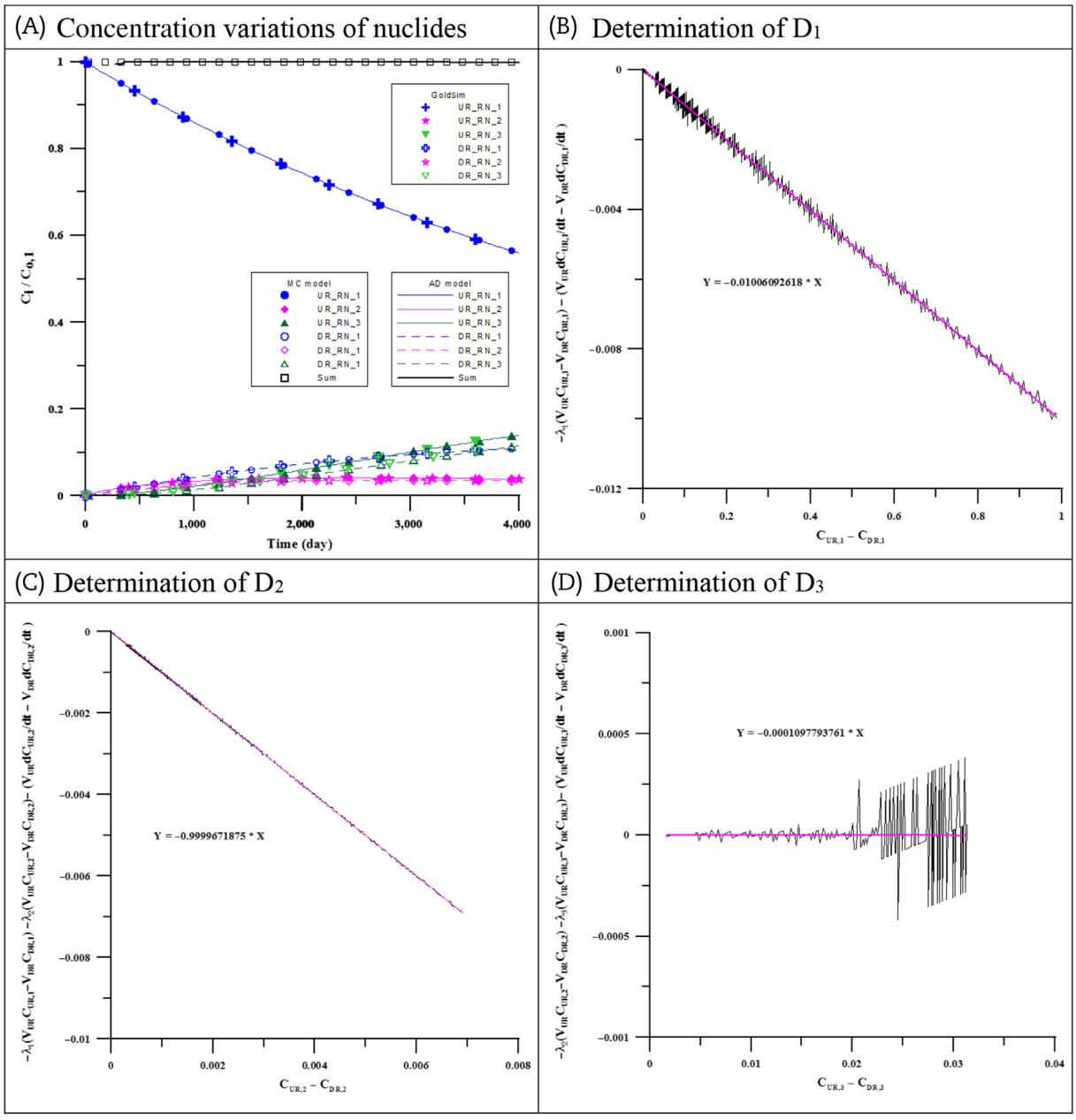

Fig. 4. Analysis of Case_S. (A) Concentration variations of nuclides. (B) Determination of D_1. (C) Determination of D_2. (D) Determination of D_3. DR, downstream reservoir; UR, upstream reservoir.

Table 2
Estimation of the diffusion coefficient (D_i) of all nuclides for the assumed cases.

	Case_S			Case_P		
	RN_1	RN_2	RN_3	RN_1	RN_2A	RN_2B
Designed D	1.000E−4	1.000E−2	1.000E−6	1.000E−6	1.000E−4	1.000E−2
Fitted slope	−1.006E−2	−1.000E+0	−1.098E−4	−1.147E−4	−9.999E−3	−9.995E−1
Estimated D	1.006E−4	1.000E−2	1.098E−6	1.147E−6	9.999E−5	9.995E−3
Deviation	0.61%	0.00%	9.78%	14.68%	0.01%	0.05%

value. The deviation of D_3 is slightly higher (9.78%). This error is acceptable, particularly for its small default value of 1E−6 cm^2/d.

3.2. Parallel reactions

The default data of parallel reactions (Case_P), shown in Table 1, are used to test the correctness of the parallel reaction solutions, which are as in Eqs. (18–20) for the continuum model and Eqs. (33–35) for the compartmental model. In Case_P, the diffusion coefficient of the parent nuclide is set at 1E−6 cm^2/d only. The stoichiometric yield factors of the product nuclides are assumed to be 0.1 and 0.9. The diffusion coefficient of the first product nuclide RN_2A is 1E−4 cm^2/d, which is smaller than the value of the second product nuclide RN_2B (D_{2B}: 1E−2 cm^2/d). The numerical diffusion

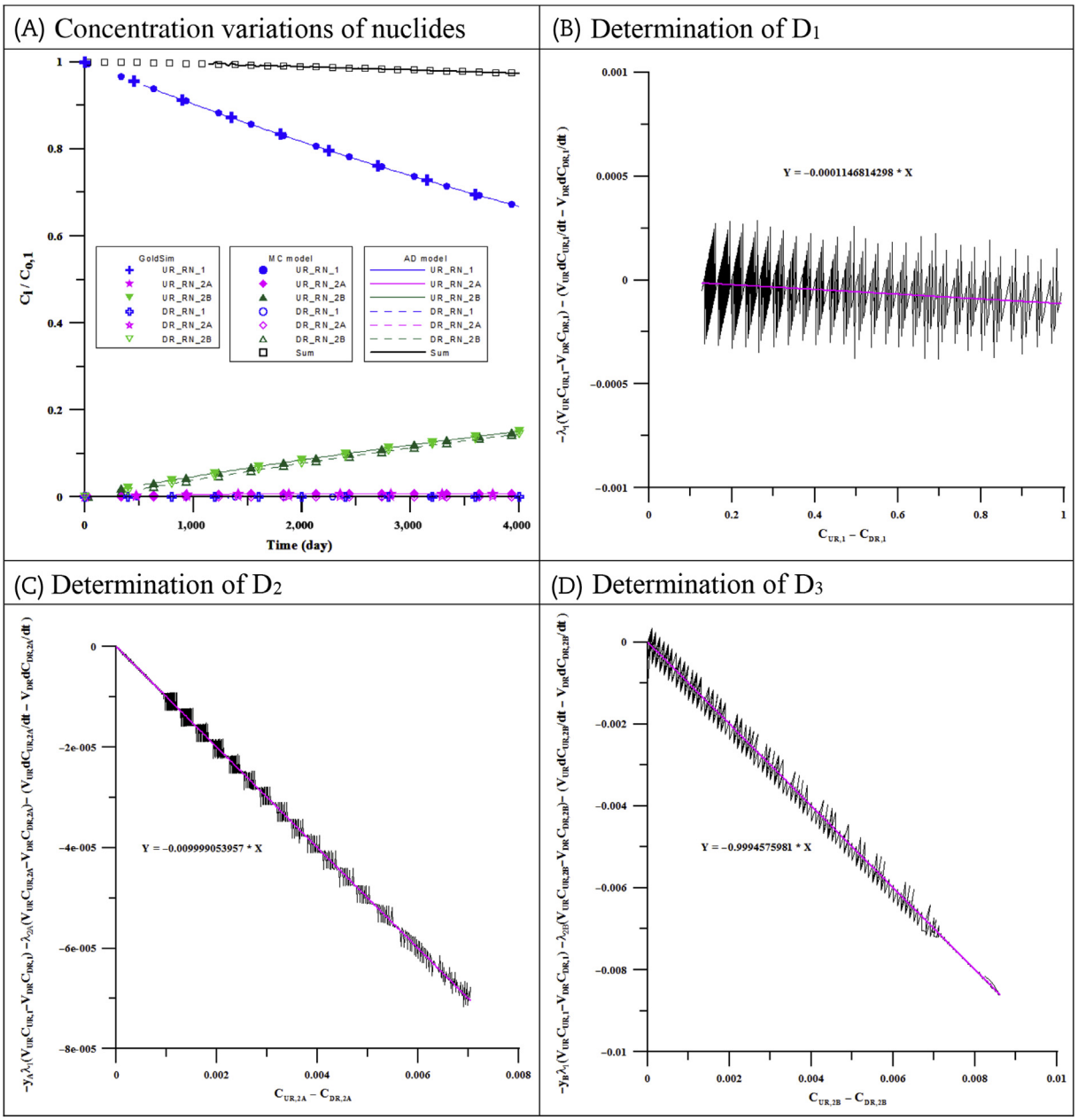

Fig. 5. Analysis of Case_P. (A) Concentration variations of nuclides. (B) Determination of D_1. (C) Determination of D_2. (D) Determination of D_3. DR, downstream reservoir; UR, upstream reservoir.

experimental results are shown in Fig. 5A. The concentrations estimated using the continuum model and compartmental model are consistent with the simulation results by GoldSim. The RN_1 concentration in the UR decreases primarily because of the decay effect of RN_1. For the low diffusion coefficient value of RN_1, the RN_1 concentration in the DR is considerably small. The product nuclide RN_2B shows a higher stoichiometric yield factor (y_B: 0.9) than that of RN_2A (y_A: 0.1). Thus, the RN_2B concentrations in the UR and DR are clearly higher than the RN_2A concentration. In addition, because RN_2B is highly diffusive, it diffuses through the specimen rapidly. The RN_2B concentration in the UR remains slightly higher than that in the DR. For a small stoichiometric yield factor, the RN_2A concentration always maintains a low value. The phenomenon of concentration variation corresponds to the default values, which show the credibility of the solutions of the parallel reactions.

Following the preceding plotting procedures for determining the diffusion coefficient of nuclides, the results of linear regression are shown in Figs. 5B–5D. In addition, the slopes show a constant value. The estimated results are listed in Table 2. The deviation of the estimated diffusion coefficient of the parent nuclide RN_1 is slightly high. However, for a small diffusion coefficient of RN_1, the estimated value of D_1 is of the same order as the theoretical value. Thus, the deviation should be accepted. The deviations of the estimated diffusion coefficients of the product nuclide RN_2A and RN_2B are extremely small.

3.3. Comparison of D_1 with Chen et al's [14] model

Because no model for determining the diffusion coefficient of the product nuclide exists in the literature, the method of estimating the diffusion coefficient of the parent nuclide was compared with that proposed by Chen et al [14]. The default data

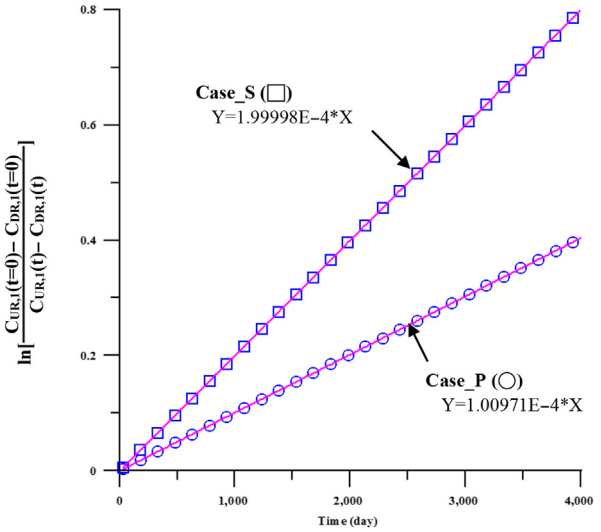

Fig. 6. Estimation of the apparent diffusion coefficient (D_1) for Case_S and Case_P, using Chen et al's [14] method. DR, downstream reservoir; UR, upstream reservoir.

Table 3
Comparison of the proposed method and Chen et al's method for estimating the D_1 of the assumed cases.

	Case_S		Case_P	
	This study	Chen's method	This study	Chen's method [14]
Designed D_1	1.000E−4	1.000E−4	1.000E−6	1.000E−6
Value of λ_1		1.000E−4		1.000E−4
Fitted slope		2.000E−4		1.010E−4
Estimated D_1	1.006E−4	1.000E−4	1.147E−06	9.710E−7
Deviation	0.61%	0.00%	14.68%	2.90%

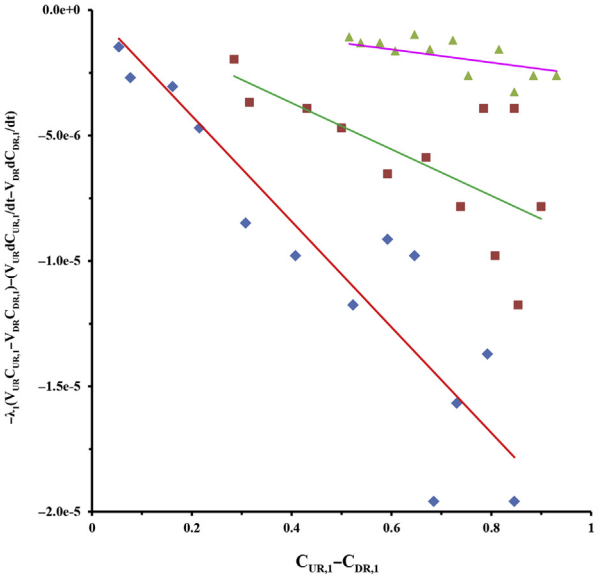

Fig. 7. Estimation of the apparent diffusion coefficient (D_1) by proposed method with identical ^{36}Cl concentration. DR, downstream reservoir; UR, upstream reservoir.

of the parent nuclide in Case_S and Case_P were used. After plotting $\ln\left[\frac{C_{A,1}(t=0)-C_{B,1}(t=0)}{C_{A,1}(t)-C_{B,1}(t)}\right]$ against time (t), an approximate constant slope (s) was acquired using linear regression (Fig. 6). The diffusion coefficients were obtained after inputting the approximate slope.

The results are shown in Table 3. Although the proposed method differed slightly from that proposed by Chen et al [14], the observed minimal deviation strongly suggests that the proposed method can be used for accurately determining the diffusion coefficient of nuclides for serial and parallel reactions.

3.4. Comparison of D_1 with experimental data

The nuclide ^{36}Cl was used as tracer to research the diffusion coefficient of varied density of compacted bentonite in a variable concentration through-diffusion experiment [15]. The volume of the inlet and outlet reservoirs is 100 mL. The densities of compacted bentonite are 1.0 g/cm^3, 1.2 g/cm^3, and 1.4 g/cm^3. The thicknesses are 0.53 cm and 0.83 cm. The experimental data of ^{36}Cl were obtained by rearranged data presented by García-Gutiérrez et al [15]; data were applied to calculate the diffusion coefficient using the proposed method. The analysis results are shown in Fig. 7 and Table 4. In Fig. 7, the rearranged data obviously distribute with an approximately linear relationship. Owing to the lack of thickness information in the experimental data shown in Fig. 1B in García-Gutiérrez et al [15], both thicknesses (0.53 cm and 0.83 cm) were used to calculate the diffusion coefficient. The estimated value in Table 4 shows results similar to those in García-Gutiérrez et al [15].

3.5. Discussion

3.5.1. Sampling frequency (Δt)

The validity and capability of the models proposed in this study were verified in the previous section. In this section, the importance of considering the sampling frequency during the experiment performance is emphasized. To analyze the sampling frequency quantitatively, the sampling period (Δt) was varied individually. Because the proposed models are not dimensionless, Case_dt− and Case_dt+, with sampling periods of 7 days and 60 days, respectively, were defined for comparison. Results from both cases are displayed in Fig. 8.

It is evident that distinct sampling frequencies have a negligible influence on the nuclide concentration variations in both UR and DR (Fig. 8A). Regarding the D_1 calculation, the high sampling frequency caused a high numerical deviation. To determine the diffusion coefficient of the product nuclide, the effect of the sampling frequency is, again, not a crucial factor (Figs. 7D and 8C). The analysis results are presented in Table 5. Case_dt+, with a longer sampling period, likely caused slightly higher deviation than the other cases, particularly for RN_3. However, a higher error was observed in the diffusion coefficient of RN_3 as a result of an extremely small default value (i.e., considerable error propagation occurred during the calculation). The difference in the effect of the sampling period in determining the diffusion coefficient is not a critical problem, according to our validity test.

3.5.2. Specimen thickness (L)

The influence of specimen thickness is shown in Fig. 9. The breakthrough curves of the parent nuclide in the DR are evidently increasing in Case_L−. This is because Case_L−, with a thinner specimen, allowed the easy diffusion of RN_1. As expected, nuclides diffusing through a thicker specimen (Case_L+) took considerably more time. Furthermore, a relatively slower diffusion as a consequence of a thicker specimen led to a significant concentration variation in both UR and DR. This explains why the distance of departure of the simulated breakthrough curves of RN_3 in the UR and DR is greater for Case_L+ than for Case_S and Case_L−.

The thicker specimen in Case_L+ seems to have a higher

Table 4
Experimental data reported by García-Gutiérrez et al (2004) [15].

Nuclide	Half-life (yr)	V_A (cm^3)	V_B (cm^3)	Diameter (mm)	Density (g/cm^3)	L (cm)	Porosity	D_a (m^2/s)	
								Ref.	This study
^{36}Cl	301000	100	100	50	1.0	0.53	0.180	1.51E−10	1.58E−10
						0.83	0.153	2.41E−10	2.91E−10
					1.2	0.53	0.105	1.03E−10	1.19E−10
						0.83	0.152	1.66E−10	1.29E−10
					1.4	0.53	0.059	4.90E−11	5.97E−11
						0.83	0.034	5.00E−11	5.51E−12

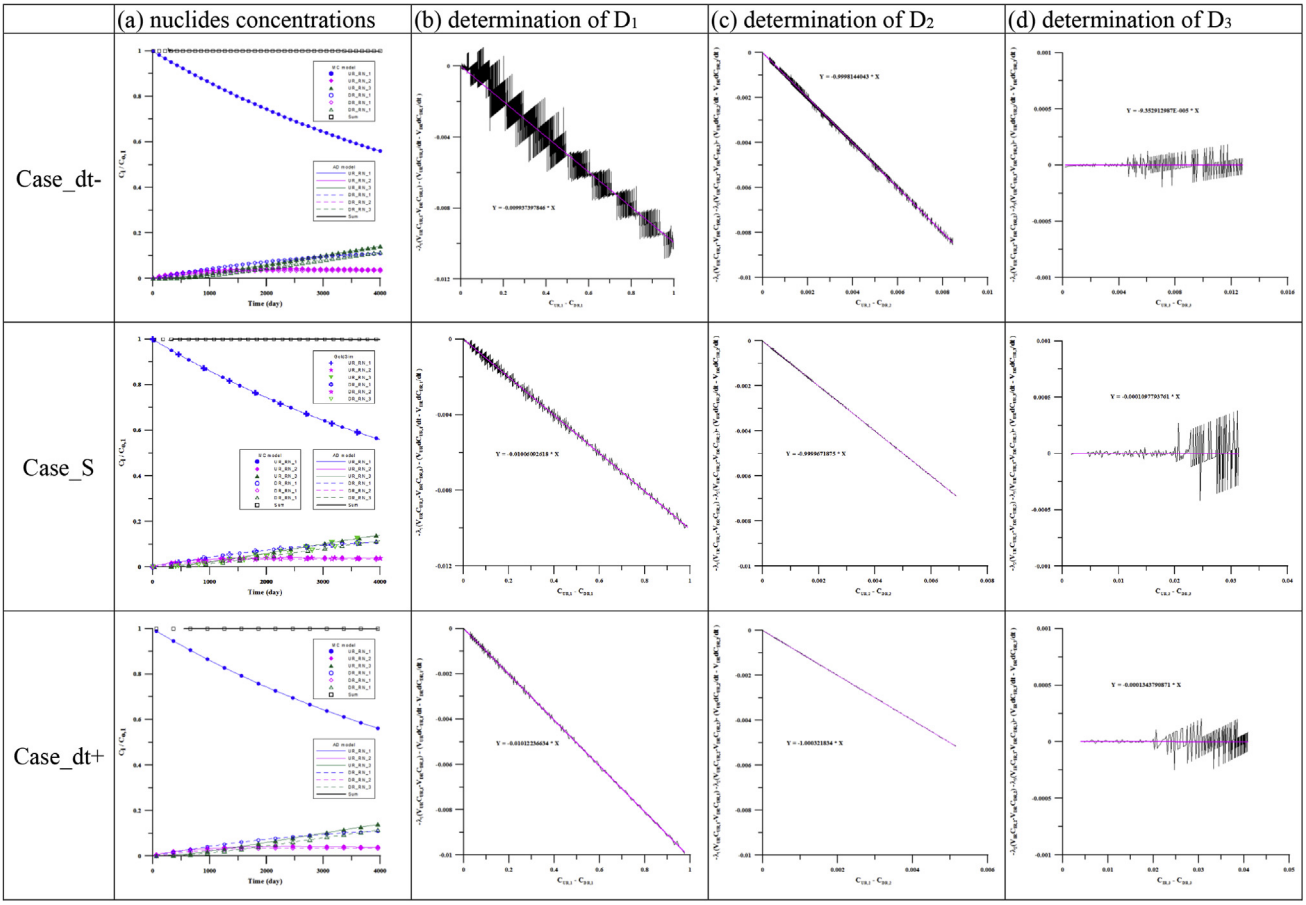

Fig. 8. Comparison of the three cases with varying sampling periods (Δt). (A) Nuclide concentrations. (B) Determination of D_1. (C) Determination of D_2. (D) Determination of D_3. DR, downstream reservoir; UR, upstream reservoir.

Table 5
Comparison of the estimated D from the cases with varying sampling periods (Δt).

Designed D	RN_1			RN_2			RN_3		
	1.000E−04			1.000E−02			1.000E−06		
	Case_dt−	Case_S	Case_dt+	Case_dt−	Case_S	Case_dt+	Case_dt−	Case_S	Case_dt+
Fitted slope	−9.937E−3	−1.006E−2	−1.012E−2	−9.998E−1	−1.000E+0	−1.000E+0	−9.353E−5	−1.098E−4	−1.344E−4
Estimated D	9.937E−5	1.006E−4	1.012E−4	9.998E−3	1.000E−2	1.000E−2	9.353E−7	1.098E−6	1.344E−6
Deviation	0.63%	0.61%	1.22%	0.02%	0.00%	0.03%	6.47%	9.78%	34.38%

deviation of the distribution, which result from numerical inversion. However, no such severe deviation is observed in the D_2 determination. The statistical results are shown in Table 6 (i.e., a smaller estimated deviation is always accompanied by a large diffusion coefficient, RN_1 or RN_2, whereas a large deviation is often accompanied by an extremely small diffusion coefficient, RN_3). Consequently, the effect of specimen thickness mainly depends on the diffusion coefficient value.

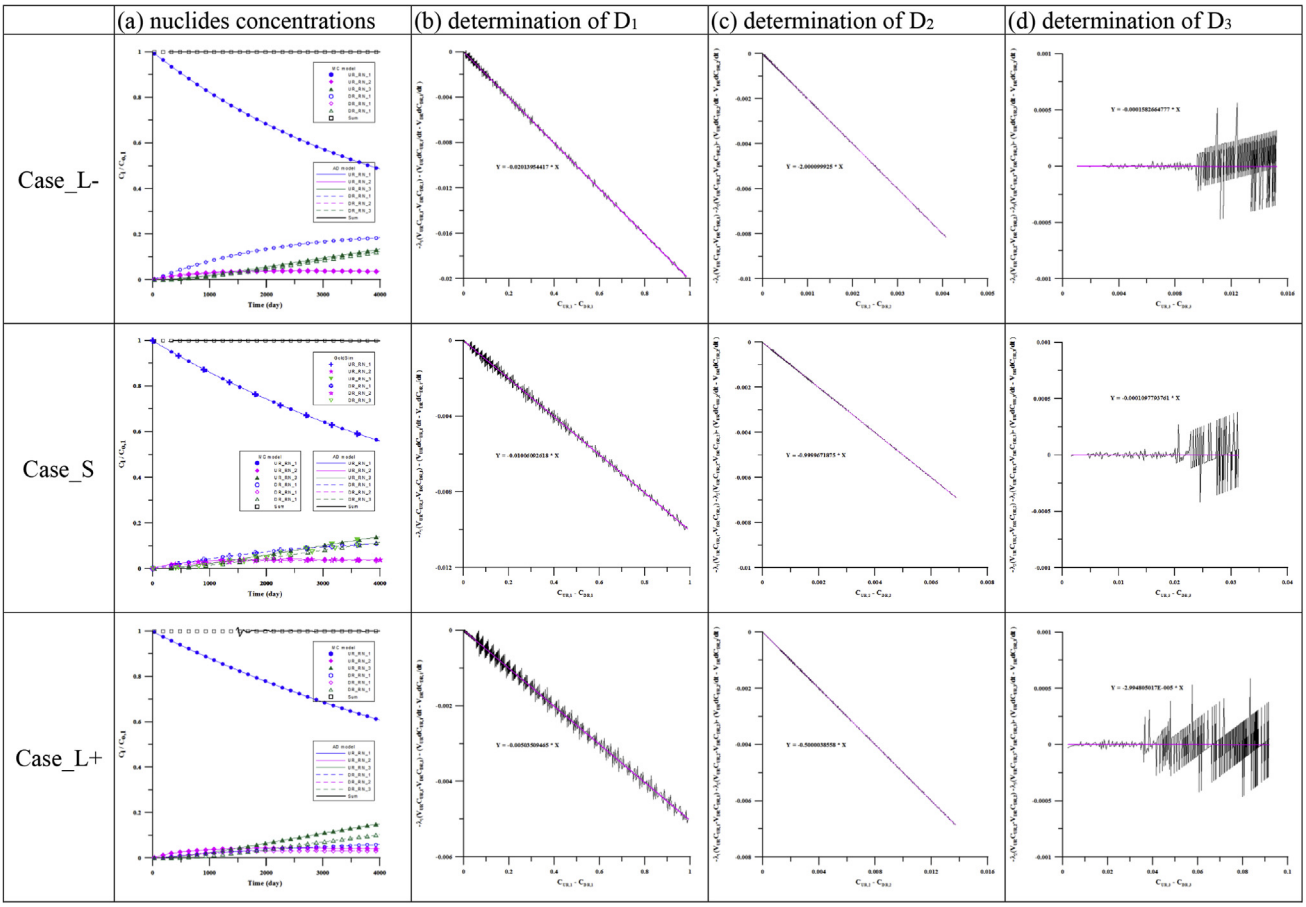

Fig. 9. Comparison of three cases with varying specimen thicknesses (L). (A) Nuclide concentrations. (B) Determination of D_1. (C) Determination of D_2. (D) Determination of D_3. DR, downstream reservoir; UR, upstream reservoir.

Table 6
Comparison of the estimated D from the cases with varying specimen thickness (L).

Designed D	RN_1			RN_2			RN_3		
	1.000E−04			1.000E−02			1.000E−06		
	Case_L−	Case_S	Case_L+	Case_L−	Case_S	Case_L+	Case_L−	Case_S	Case_L+
Fitted slope	−2.014E−2	−1.006E−2	−5.035E−3	−2.000E+0	−1.000E+0	−5.000E−1	−1.583E−4	−1.098E−4	−2.995E−5
Estimated D	1.007E−4	1.006E−4	1.007E−4	1.000E−2	1.000E−2	1.000E−2	7.913E−7	1.098E−6	5.990E−7
Deviation	0.70%	0.61%	0.70%	0.00%	0.00%	0.00%	20.87%	9.78%	40.10%

4. Limitations and conclusion

The methodology for determining the diffusion coefficient for the sequentially reactive nuclide through-diffusion model is limited to a first-order decay chain. In addition, it only calculates the diffusion coefficient of a single parent nuclide. Furthermore, all calculations are conducted based on the assumption that the concentration gradient inside the specimen is constant. This means that the proposed method should be used to consider conditions involving either an extremely thin specimen or an extremely long period of diffusion time for nuclides possessing extremely small diffusion coefficients. This method can be extremely powerful, particularly when a diffusion experiment is conducted with an extremely thin specimen, a long diffusion time, and a parent nuclide with a fast decay constant.

As a matter of fact, planning of a through-diffusion experiment for a multimember decay chain is underway, although it may take longer than we might expect to perform the experiment to obtain the diffusion coefficients. Therefore, the data obtained from the experiment and the model prediction will be compared and verified for our next study.

Conflicts of interest

All authors have no conflicts of interest to declare.

References

[1] I. Neretnieks, Diffusion in the rock matrix: an important factor in radionuclide retardation, J. Geophys. Res. 85 (1980) 4379–4397.
[2] M. García-Gutiérrez, J.L. Cormenzana, T. Missanal, M. Mingarro, J. Molinero, Overview of laboratory methods employed for obtaining diffusion coefficients in FEBEX compacted bentonite, J. Iberian Geol. 32 (2006) 37–53.
[3] C.D. Shackelford, Laboratory diffusion testing for waste disposal – a review, J. Contam. Hydrol. 7 (1991) 177–217.
[4] M. Zhang, M. Takeda, H. Nakajima, Strategies for solving potential problems associated with laboratory diffusion and batch experiments—part 1. An

overview of conventional test methods, in: WM'06 Conference, Tucson, AZ, 2006.
[5] M. Takeda, H. Nakajima, M. Zhang, T. Hiratsuka, Laboratory longitudinal diffusion tests: 1. Dimensionless formulations and validity of simplified solutions, J. Contam. Hydrol. 97 (2008) 117–134.
[6] M. Takeda, M. Zhang, H. Nakajima, Strategies for solving potential problems associated with laboratory diffusion and batch experiments–part 2. Future improvements, in: WM'06 Conference, Tucson, AZ, 2006.
[7] M. Zhang, M. Takeda, H. Nakajima, Determining the transport properties of rock specimens using an improved laboratory through-diffusion technique, MRS Proc. 932 (2006) 113.1. http://dx.doi.org/10.1557/PROC-932-113.1.
[8] H.S. Carslaw, J.C. Jaeger, Conduction of Heat in Solids, second ed., Oxford University Press, New York, 1959.
[9] J. Crank, The Mathematics of Diffusion, second ed., Clarendon, Oxford, UK, 1975.
[10] W.F. Brace, J.B. Walsh, W.T. Frangos, Permeability of granite under high pressure, J. Geophys. Res. 73 (1968) 2225–2236.
[11] X. Lü, J. Ahl, Studying of salt diffusion coefficient in brick: analytical and numerical methods, J. Mater. Sci. 40 (2005) 3795–3802.
[12] G.J. Moridis, Semianalytical solutions for parameter estimation in diffusion cell experiments, Water Resour. Res. 35 (1999) 1729–1740.
[13] T.V. Bharat, P.V. Suvapullaiah, M.M. Allam, Swarm intelligence-based solver for parameter estimation of laboratory through-diffusion transport of contaminants, Comput. Geotechnics 36 (2009) 984–992.
[14] C.L. Chen, T.H. Wang, C.H. Lee, S.P. Teng, The development of a through-diffusion model with a parent–daughter decay chain, J. Contam. Hydrol. 138–139 (2012) 1–14.
[15] M. García-Gutiérrez, J.L. Cormenzana, T. Missanal, M. Mingarro, Diffusion coefficients and accessible porosity for HTO and ^{36}Cl in compacted FEBEX bentonite, Appl. Clay Sci. 26 (2004) 65–73.